Int. J. Solids Structures Vol. 27, No. 5, pp. 601–628, 1991
Printed in Great Britain.

0020–7683/91 $3.00+.00

PERTURBATION ANALYSIS OF THERMOVISCOPLASTIC INSTABILITIES IN BIAXIAL LOADING

DANIEL DUDZINSKI and ALAIN MOLINARI
L.P.M.M., U.A. no. 1215, Faculté des Sciences, Ile du Saulcy, 57045 Metz Cedex 01, France

(*Received* 21 *June* 1989; *in revised form* 23 *January* 1990)

Abstract—The sheet metal ductility for a thermoviscoplastic material is analysed by using a perturbation method. A significant rate of growth of the instability is characterized in terms of an effective instability analysis. Analytical results are obtained for quite general material behavior (including time-dependent effects). They match the results of Hill (1952, *J. Mech. Phys. Solids* **1**, 19) and Stören and Rice (1975, *J. Mech. Phys. Solids* **23**, 421) for time-independent behavior.

1. INTRODUCTION

Sheet metal ductility is limited by plastic instabilities, especially by necking and shear bands. The theoretical analysis of sheet necking usually considers two modes of plastic instability, namely the diffuse necking and the localized necking modes. The maximum allowable strains are determined by localized necking, and consequently diffuse necking has less practical interest.

The first analysis of localized necking was developed by Hill (1952) for rigid-plastic materials obeying the J_2-flow theory. However, this analysis predicts an infinite ductility in biaxial stretching while experiments show that necking-type failures take place.

To resolve this discrepancy two approaches have been developed. The first is the M.K. defect theory of Marciniak and Kuczynski (1967), where an initial defect in the form of a thin groove is postulated. The second approach relies on a bifurcation analysis and a J_2 rate-independent deformation theory which introduces in a simple way an effect similar to a pointed vertex on the yield loci, promoting instability in biaxial tension (Stören and Rice, 1975).

A two-zone defect approach has also been developed by Ferron and Mliha-Touati (1985) for small defects. Thus, the equations can be linearized and an analytical solution of the problem is obtained.

An alternative approach is based on perturbation analysis (Dudzinski and Molinari, 1988; Canova *et al.*, 1987). The sheet is assumed to be initially homogeneous. At any stage of the postulated homogeneous deformation process, a perturbation is superimposd to the basic homogeneous flow. The flow instability or stability is characterized by the fact that the perturbation is increasing or decreasing. The method can be used for the analysis of either diffuse necking or localized necking. Indeed, it has been quite successfully developed in fluid mechanics and later on used in solids mechanics for shear band analysis (Clifton, 1978; Bai, 1982; Molinari, 1985; Fressengeas and Molinari, 1987), and for necking in uniaxial tension (Fressengeas and Molinari, 1985). It will be shown that the perturbation analysis combines the main advantages of both the M.K. analysis and the bifurcation theory. Moreover, the gap existing between these two theories can be overcome.

The perturbation approach shows that an unstable behavior does occur for a limit strain depending on the strain path. This instability is activated even for an equibiaxially stretched rate-independent material obeying a flow law with a smooth yield surface, in agreement with the M.K. analysis. However, for a rate-independent material with a smooth yield surface, no band mode bifurcation is predicted under equibiaxial stretching by the classical analysis of Hill (1952) and Stören and Rice (1975). This apparent contradiction can be enlightened by the analysis of the rate of growth of the unstable modes. In cases where no bifurcation is predicted by the classical analysis, instability is nevertheless not

precluded, but the growth of the unstable modes appears to be very low. On the contrary, very fast growing modes exist when a bifurcation appears. Therefore, the link between the M.K. and the bifurcation approaches can be provided by the analysis of the rate of growth of infinitesimal perturbations. For rate-independent materials, a complete agreement is then obtained with the bifurcation results of Hill (1952), Stören and Rice (1975), and Hutchinson and Neale (1978).

An advantage of the perturbation analysis relies on the fact that quite general material behavior can be accounted for. Thus, in this paper, the effects of rate sensitivity, material anisotropy, and heat conduction are discussed. Inertia can also be analysed. In contrast, only rate-independent behavior can be addressed by the bifurcation analysis while heat conduction and inertia effects cannot be taken into account in the two-zone M.K. analysis or in the analytical linearized defect theory of Ferron and Mliha-Touati (1985).

The necking mode instability in a heat conducting rigid anisotropic thermoviscoplastic material is analysed here. The governing equations are settled in Section 2. In Section 3, the general features of the linearized analysis are presented. An application to an isotropic material under isothermal conditions is considered in Section 4. An important point comes from the observation that the first mode to be activated is not necessarily the dominant mode leading to localized necking. Actually, this mode may present a slow rate of growth and can be overcome by a fast mode which is activated later, but with a much higher rate of growth. Therefore, there is a need to evaluate in some way the rate of growth of the different modes and to select the dominant modes governing the instability process. In order to achieve this, a concept of effective instability is proposed. While the onset of instability is characterized by a classical instability analysis (herein named absolute instability analysis), the effective instability analysis characterizes the overall strains for which a certain intensity in the instability growth is developed. The effective instability is then used to analyse thermal effects in sheet metal forming (Section 5) and material anisotropy (Section 6). Finally, the effect of a pointed vertex on the yield surface at the loading point is discussed in Section 7.

The ductility of metal sheets is characterized by forming limit curves. All the results are obtained in simple analytical forms where the role of the physical parameters can be easily discussed.

2. GOVERNING EQUATIONS

The process of localized sheet necking in biaxial loading is analysed within the framework of generalized plane stress. The principal axes of strain rates are designated by X and

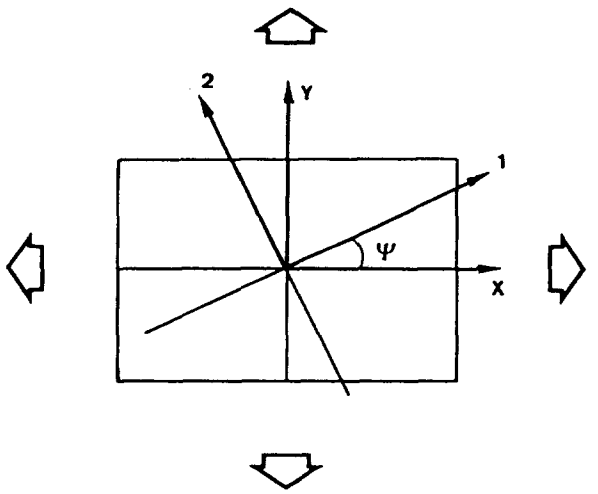

Fig. 1. Geometry of the sheet plane. The directions of the overall principal strain rate are X and Y. The principal axes of orthotropy coincide with the directions X and Y up to instability.

Y (Fig. 1). Due to the plane stress assumption the non-vanishing components of the stress tensor, in any frame (x_1, x_2) defined in the sheet plane, are:

$$\sigma_{11} = \sigma_1; \quad \sigma_{22} = \sigma_2 \quad \text{and} \quad \sigma_{12}.$$

The strain rates, as well as the stress components, are considered as uniform through the thickness of the plate.

It is supposed that loading conditions are always satisfied (i.e. elastic unloading is disregarded). Thus, since large deformations are considered, elasticity can be neglected.

The material behavior is stated to be rigid viscoplastic. The associated flow law is given by:

$$D_{\alpha\beta} = \dot{\lambda} \frac{\partial \bar{\sigma}}{\partial \sigma_{\alpha\beta}}. \tag{1}$$

The Eulerian strain-rate tensor $D_{\alpha\beta}$ is defined by:

$$D_{\alpha\beta} = \tfrac{1}{2}(v_{\alpha,\beta} + v_{\beta,\alpha}); \quad \alpha, \beta = 1, 2 \tag{2}$$

where v_α are the velocity components, and $,\alpha$ designates the partial derivative with respect to x_α.

The material is assumed to present an orthotropic symmetry, and the principal axes of anisotropy (x, y) coincide with the principal axes of strain rate (X, Y) as long as the deformation is uniform.

The equivalent stress, in the Hill theory of orthotropic plastic materials (1950), is given by:

$$\bar{\sigma} = \sqrt{\frac{3}{2}} \left[\frac{(G+H)\sigma_{xx}^2 - 2H\sigma_{xx}\sigma_{yy} + (H+F)\sigma_{yy}^2 + N\sigma_{xy}^2 + N\sigma_{yx}^2}{F+G+H} \right]^{1/2} \tag{3}$$

where F, G, H and N are parameters characterizing the current state of anisotropy. They can be deduced from the ratio R_ϕ of the transverse to the through-thickness strain (see Appendix A). The components σ_{xx}, σ_{yy} and σ_{xy} are referred to the principal axis of anisotropy. The equivalent strain rate $\dot{\bar{\varepsilon}}$ is work-conjugated to the equivalent stress $\bar{\sigma}$:

$$\sigma_{ij} D_{ij} = \bar{\sigma} \dot{\bar{\varepsilon}}. \tag{4}$$

From the definition of $\dot{\bar{\varepsilon}}$ (4) and the fact that $\bar{\sigma}$ is a homogeneous function of degree 1 in the components σ_{ij}, it results, after substitution of the flow law (1) into (4), that:

$$\dot{\lambda} = \dot{\bar{\varepsilon}}. \tag{5}$$

After some algebraic manipulations of (1) it can be shown that:

$$\dot{\bar{\varepsilon}} = \sqrt{\frac{2}{3}} [F+G+H]^{1/2} \left[F\left(\frac{GD_{yy} - HD_{zz}}{FG+GH+HF}\right)^2 + G\left(\frac{HD_{zz} - FD_{xx}}{FG+GH+HF}\right)^2 + H\left(\frac{FD_{xx} - GD_{yy}}{FG+GH+HF}\right)^2 + 2\frac{D_{xy}^2}{N} \right]^{1/2}. \tag{6}$$

The hardening law is stated to a power law relating the equivalent stress $\bar{\sigma}$ to the absolute temperature θ, the equivalent strain rate $\dot{\bar{\varepsilon}}$ and the cumulated plastic strain $\bar{\varepsilon}$:

$$\bar{\sigma} = \mu \bar{\varepsilon}^n \dot{\bar{\varepsilon}}^m \theta^\nu$$

$$\bar{\varepsilon} = \int_0^t \dot{\bar{\varepsilon}}(\tau)\, d\tau. \tag{7}$$

The material characteristics are the constant μ, the strain hardening exponent n, the strain rate sensitivity parameter m and the thermal softening exponent ν ($\nu < 0$).

The flow law expressed in the axes (X, Y) reads:

$$D_{xx} = T_{xx}\dot{\bar{\varepsilon}}; \quad D_{yy} = T_{yy}\dot{\bar{\varepsilon}}; \quad D_{xy} = T_{xy}\dot{\bar{\varepsilon}} \tag{8}$$

with

$$T_{xx} = \frac{3}{2}\frac{(G+H)\sigma_{xx} - H\sigma_{yy}}{F+G+H}\frac{1}{\bar{\sigma}} = \frac{\partial\bar{\sigma}}{\partial\sigma_{xx}}$$

$$T_{yy} = \frac{3}{2}\frac{(H+F)\sigma_{yy} - H\sigma_{xx}}{F+G+H}\frac{1}{\bar{\sigma}} = \frac{\partial\bar{\sigma}}{\partial\sigma_{yy}}$$

$$T_{xy} = \frac{3}{2}\frac{N\sigma_{xy}}{F+G+H}\frac{1}{\bar{\sigma}} = \frac{\partial\bar{\sigma}}{\partial\sigma_{xy}}. \tag{9}$$

In the following, the equations have to be expressed in a frame (x_1, x_2) having an orientation angle Ψ with respect to (X, Y) (Fig. 1).

The flow law, written in the (x_1, x_2) frame, is:

$$D_{11} = T_{11}\dot{\bar{\varepsilon}}; \quad D_{22} = T_{22}\dot{\bar{\varepsilon}}; \quad D_{12} = T_{12}\dot{\bar{\varepsilon}} \tag{10}$$

with

$$T_{11} = T_{xx}\cos^2\Psi + T_{yy}\sin^2\Psi + 2T_{xy}\sin\Psi\cos\Psi$$

$$T_{22} = T_{xx}\sin^2\Psi + T_{yy}\cos^2\Psi - 2T_{xy}\sin\Psi\cos\Psi$$

$$T_{12} = -(T_{xx} - T_{yy})\sin\Psi\cos\Psi + T_{xy}(\cos^2\Psi - \sin^2\Psi). \tag{11}$$

Under the plane stress assumption, the compatibility conditions are (with the usual approximations done in the plane stress condition):

$$\frac{1}{2}\left(\frac{\partial^2 D_{11}}{\partial x_2^2} + \frac{\partial^2 D_{22}}{\partial x_1^2}\right) = \frac{\partial^2 D_{12}}{\partial x_1\,\partial x_2}. \tag{12}$$

The current thickness is h. Then the equilibrium equations read:

$$\frac{\partial}{\partial x_\alpha}(h\sigma_{\alpha\beta}) = 0; \quad \alpha, \beta = 1, 2 \tag{13}$$

where σ_{11}, σ_{22} and σ_{12} denote the values of the stress components averaged through the thickness (Hill, 1950). The current thickness is related to the initial homogeneous thickness $h(0)$ by the relation:

$$h = h(0)\,e^{\varepsilon_3} \tag{14}$$

where ε_3 is the logarithmic deformation in the direction x_3 orthogonal to the plate. The relation (14) is equivalent to:

$$\dot{h}/h = D_{33}. \tag{15}$$

Assuming that a fraction β (Taylor–Quinney coefficient) of the plastic work is converted into heat, and that the boundaries of the plate are adiabatic, then the conservation of energy leads to the following equation (see Appendix B):

$$c\dot{\theta} = k\left(\frac{\partial^2\theta}{\partial x_1^2} + \frac{\partial^2\theta}{\partial x_2^2}\right) + \frac{k}{h}\left(\frac{\partial\theta}{\partial x_1}\frac{\partial h}{\partial x_1} + \frac{\partial\theta}{\partial x_2}\frac{\partial h}{\partial x_2}\right) + \beta\bar{\sigma}\dot{\bar{\varepsilon}}. \tag{16}$$

$\dot{\theta}$ is the material derivative of the absolute temperature, c is the heat capacity and k is the thermal conductivity. The Taylor–Quinney coefficient will be taken equal to 0.9.

With the incompressibility condition:

$$D_{11} + D_{22} + D_{33} = 0 \tag{17}$$

a complete set of 11 equations is obtained: the flow law (10), the hardening law (7), the energy equation (16), the compatibility and the equilibrium (12, 13), the definition of the equivalent stress (3), the incompressibility condition (17) and relation (15). The unknowns are, for a given Ψ: the strain rates D_{11}, D_{22}, D_{12} and D_{33}, the stresses σ_{11}, σ_{22}, σ_{12} and $\bar{\sigma}$, the strain rate $\dot{\bar{\varepsilon}}$, the temperature θ and the thickness h.

Overall constant principal strain rates D°_{xx} and D°_{yy} [in the frame (X, Y)] are applied at remote boundaries. The straining path is linear and defined by the ratio:

$$\frac{D^\circ_{yy}}{D^\circ_{xx}} = \rho = \text{const.} \tag{18}$$

The following velocity field (defined modulo arbitrary additive constants)

$$\begin{aligned} v_x &= xD^\circ_{xx} \\ v_y &= yD^\circ_{yy} \end{aligned} \tag{19}$$

is a solution of (18). As long as the flow is stable, the velocity field is given by (19) and the strain rates are uniform. Inertia is neglected.

The initial temperature and thickness are uniform: $\theta = \theta^\circ(0)$, $h = h^\circ(0)$. A homogeneous solution, denoted by the superscript $^\circ$, $\mathbf{S}^\circ = (D^\circ_{11}, D^\circ_{22}, \ldots, \theta^\circ)$ results from these conditions. In particular, the homogeneous principal stresses satisfy the following relation, resulting from (3):

$$\frac{\sigma^\circ_{xx}}{\bar{\sigma}^\circ} = \sqrt{\frac{2}{3}}\left[\frac{F+G+H}{G+H-2H\alpha+(H+F)\alpha^2}\right]^{1/2} \tag{20}$$

where the stress ratio α is defined by:

$$\alpha = \frac{\sigma^\circ_{yy}}{\sigma^\circ_{xx}} = \frac{\rho(G+H)+H}{(H+F)+H\rho}. \tag{21}$$

The second equality in (21) comes from the flow law (8).

Therefore, when the flow is stable, T_{xx}, T_{yy} and T_{xy} depend only on the material constants F, G, H and N, and the loading path ρ, while the coefficients T_{ij} also depend on the orientation Ψ of the frame (x_1, x_2).

3. EFFECTIVE INSTABILITY ANALYSIS

The stability of the homogeneous solution is now analysed. Since the localized mode of necking presents the most practical interest, the analysis is restricted to that mode. The stability of the homogeneous solution $\mathbf{S}^\circ$ is tested by superposition at any time t_0 of a small perturbation $\delta\mathbf{S} = (\delta D_{11}, \delta D_{22}, \ldots, \delta\theta)$.

The following form is stated for the components of $\delta\mathbf{S}$:

$$\delta S_i = \delta S_i^0 \exp[\eta(t-t_0)] \exp(i\xi x_1). \tag{22}$$

The perturbation is constant on lines $x_1 = \text{const.}$ of inclination Ψ (Fig. 1). The polarization vector of the perturbation is:

$$\delta \mathbf{S}^0 = (\delta D_{11}^0, \delta D_{22}^0, \ldots, \delta\theta^0). \tag{23}$$

The spatial modulation is periodic and defined by the wave number ξ. The number η (generally complex, but real in the applications considered herein) characterizes the growth of the perturbation if $\mathrm{Re}(\eta) > 0$ (instability), or the decay if $\mathrm{Re}(\eta) < 0$ (stability). When instability is occurring the growth of the perturbation is viewed to represent the early stages of a necking process in bands of inclination Ψ. The angle Ψ has to be optimized in a way which will be determined later. The physical solution is the real part of

$$\mathbf{S} = \mathbf{S}^0 + \delta \mathbf{S}^0 \exp[\eta(t-t_0)] \exp(i\xi x_1). \tag{24}$$

After linearization of the equations, the polarization vector $\delta \mathbf{S}^0$ appears to be an eigenvector of the following system of equations, resulting from the flow law (10):

$$\begin{aligned}
\frac{\delta D_{11}^0}{\dot{\bar{\varepsilon}}^0} &= T_{11} \frac{\delta \dot{\bar{\varepsilon}}^0}{\dot{\bar{\varepsilon}}^0} + U_{1111}^0 \frac{\delta \sigma_{11}^0}{\bar{\sigma}^0} + U_{1122}^0 \frac{\delta \sigma_{22}^0}{\bar{\sigma}^0} + 2U_{1112}^0 \frac{\delta \sigma_{12}^0}{\bar{\sigma}^0} \\
\frac{\delta D_{22}^0}{\dot{\bar{\varepsilon}}^0} &= T_{22} \frac{\delta \dot{\bar{\varepsilon}}^0}{\dot{\bar{\varepsilon}}^0} + U_{2211}^0 \frac{\delta \sigma_{11}^0}{\bar{\sigma}^0} + U_{2222}^0 \frac{\delta \sigma_{22}^0}{\bar{\sigma}^0} + 2U_{2212}^0 \frac{\delta \sigma_{12}^0}{\bar{\sigma}^0} \\
\frac{\delta D_{12}^0}{\dot{\bar{\varepsilon}}^0} &= T_{12} \frac{\delta \dot{\bar{\varepsilon}}^0}{\dot{\bar{\varepsilon}}^0} + U_{1211}^0 \frac{\delta \sigma_{11}^0}{\bar{\sigma}^0} + U_{1222}^0 \frac{\delta \sigma_{22}^0}{\bar{\sigma}^0} + (U_{1212}^0 + U_{1221}^0) \frac{\delta \sigma_{12}^0}{\bar{\sigma}^0};
\end{aligned} \tag{25}$$

from the hardening law (7):

$$\hat{\eta} \frac{\delta \bar{\sigma}}{\bar{\sigma}^0} = \left(\frac{n}{\bar{\varepsilon}^0} + n\hat{\eta} \right) \frac{\delta \dot{\bar{\varepsilon}}^0}{\dot{\bar{\varepsilon}}^0} + \nu \hat{\eta} \frac{\delta \theta^0}{\theta^0}; \tag{26}$$

from the energy equation (16):

$$-(Q+\hat{\eta})\nu \frac{\delta \theta^0}{\theta^0} + B \frac{\delta \dot{\bar{\varepsilon}}^0}{\dot{\bar{\varepsilon}}^0} + B \frac{\delta \bar{\sigma}^0}{\bar{\sigma}^0} = 0; \tag{27}$$

from the compatibility (12):

$$\delta D_{22}^0 = 0; \tag{28}$$

from the equilibrium (13) [eqn (15) has been used to eliminate the thickness h]:

$$\begin{aligned}
\hat{\eta} \frac{\delta \sigma_{11}^0}{\bar{\sigma}^0} + \frac{\sigma_{11}^0}{\bar{\sigma}^0} \frac{\delta D_{33}^0}{\dot{\bar{\varepsilon}}^0} &= 0 \\
\hat{\eta} \frac{\delta \sigma_{12}^0}{\bar{\sigma}^0} + \frac{\sigma_{12}^0}{\bar{\sigma}^0} \frac{\delta D_{33}^0}{\dot{\bar{\varepsilon}}^0} &= 0;
\end{aligned} \tag{29}$$

from the definition of the equivalent stress (3):

$$\frac{\delta\bar{\sigma}^{\circ}}{\bar{\sigma}^{\circ}} = T^{\circ}_{11}\frac{\delta\sigma^{\circ}_{11}}{\bar{\sigma}^{\circ}} + T^{\circ}_{22}\frac{\delta\sigma^{\circ}_{22}}{\bar{\sigma}^{\circ}} + 2T^{\circ}_{12}\frac{\delta\sigma^{\circ}_{12}}{\bar{\sigma}^{\circ}}; \tag{30}$$

and from the incompressibility condition:

$$\delta D^{\circ}_{11} + \delta D^{\circ}_{22} + \delta D^{\circ}_{33} = 0. \tag{31}$$

The following non-dimensional parameters have been introduced:

$$B = \frac{\beta v\bar{\sigma}^{\circ}}{c\theta^{\circ}}; \quad Q = \frac{k\xi^{\circ 2}}{c\dot{\bar{\varepsilon}}^{\circ}}; \quad \hat{\eta} = \frac{\eta}{\dot{\bar{\varepsilon}}^{\circ}}. \tag{32}$$

The parameter Q characterizes the effect of heat conduction. When the heat conductivity k is large or when the applied strain rates are small, then Q is large and the problem is isothermal. On the contrary, for small values of Q, the heat conduction effects are negligible. The coefficients T°_{ij} and U°_{ijkl} are defined by (11) and in Appendix C, respectively.

Equations (26) and (27) are obtained from the approximation of the material derivatives $\dot{\theta}$ and $\dot{\bar{\varepsilon}}$ by the partial time derivatives. This approximation is valid if the velocities are not too large.

The perturbed solution (24) does exist if the linear system (25)–(31) admits a non-zero solution δS°. Setting the determinant of that system equal to zero, the following cubic equation in $\hat{\eta}$ is obtained:

$$\begin{aligned}
&-\hat{\eta}^3 U^{\circ}_{2222}(mU^{\circ}_{2222} + T^{\circ 2}_{22}) + \hat{\eta}^2\Big[(A^{\circ}_3 - QU^{\circ}_{2222})(mU^{\circ}_{2222} + T^{\circ 2}_{22}) \\
&+ BU^{\circ}_{2222}(T^{\circ 2}_{22} - U^{\circ}_{2222}) - \frac{n}{\dot{\bar{\varepsilon}}^{\circ}}U^{\circ 2}_{2222} + A^{\circ}_1 A^{\circ}_2\Big] \\
&+ \hat{\eta}\Big[A^{\circ}_3 B(U^{\circ}_{2222} - T^{\circ 2}_{22}) + A^{\circ}_3 Q(mU^{\circ}_{2222} + T^{\circ 2}_{22}) \\
&+ \frac{n}{\dot{\bar{\varepsilon}}^{\circ}}U^{\circ}_{2222}(A^{\circ}_3 - QU^{\circ}_{2222}) + A^{\circ}_1 A^{\circ}_2(Q - B)\Big] - A^{\circ}_3 Q\frac{n}{\dot{\bar{\varepsilon}}^{\circ}}U^{\circ}_{2222} = 0
\end{aligned} \tag{33}$$

with

$$\begin{aligned}
A^{\circ}_1 &= \frac{\sigma^{\circ}_{11}}{\bar{\sigma}^{\circ}}(T^{\circ}_{11}U^{\circ}_{2222} - T^{\circ}_{22}U^{\circ}_{2211}) + \frac{2\sigma^{\circ}_{12}}{\bar{\sigma}^{\circ}}(T^{\circ}_{12}U^{\circ}_{2222} - T^{\circ}_{22}U^{\circ}_{2212}) \\
A^{\circ}_2 &= T^{\circ}_{11}U^{\circ}_{2222} - T^{\circ}_{22}U^{\circ}_{1122} \\
A^{\circ}_3 &= \frac{\sigma^{\circ}_{11}}{\bar{\sigma}^{\circ}}(U^{\circ}_{1111}U^{\circ}_{2222} - U^{\circ}_{1122}U^{\circ}_{2211}) + \frac{2\sigma^{\circ}_{12}}{\bar{\sigma}^{\circ}}(U^{\circ}_{1112}U^{\circ}_{2222} - U^{\circ}_{1122}U^{\circ}_{2212}).
\end{aligned} \tag{34}$$

To each of the three complex roots of (33) is associated a mode of perturbation. The linearized theory predicts instability (i.e. the growth of the perturbation) when one of the roots of (33) has a positive real part:

$$\mathrm{Re}(\hat{\eta}) > 0. \tag{35}$$

However, an unstable mode can sometimes grow very slowly and can therefore be overcome by another mode appearing later with a much higher rate of growth. Thus, it is useful to introduce some measure of the mode growth, in order to select the dominant modes.

Let us consider a given orientation Ψ of the perturbation, a given path of deformation ρ and a given positive number e. The values (if they exist) $\varepsilon^{c}_{x}(e, \Psi, \rho)$ and $\varepsilon^{c}_{y}(e, \Psi, \rho)$ of the

principal homogeneous logarithmic deformations are considered, for which one of the roots $\dot{\eta}$ satisfies the relation

$$\mathrm{Re}\,(\dot{\eta}) = e \tag{36}$$

while the real parts of the other roots are less than e. When the condition (36) is realized, the mode associated to the orientation Ψ is said to present an effective instability of intensity e, or an effective e-instability.

The first mode to attain the effective e-instability is characterized by the orientation Ψ^e minimizing ε_x^c. We note:

$$\begin{aligned}\varepsilon_x^c(e,\rho) &= \inf_{\Psi} \varepsilon_x^c(e,\Psi,\rho)\\ &= \varepsilon_x^c(e,\Psi^e,\rho).\end{aligned} \tag{37}$$

The onset of instability corresponds to $e = 0$; then (36) is named the absolute instability criterion. The critical strain where absolute instability occurs is named the absolute limit strain and is defined by:

$$\varepsilon_x^a = \inf_{\Psi} \varepsilon_x^c(0,\Psi,\rho). \tag{38}$$

For $e > 0$, ε_x^c is named the e-effective limit strain and Ψ^e the e-effective optimal orientation.

The parameter e introduced in the effective instability analysis is a measure of the rate of growth of the fastest mode. Indeed, among all the unstable modes, the one which is the first to attain a growth rate equal to e is selected. The corresponding effective critical strain ε_x^c can be roughly viewed as the strain for which the instability develops a growth rate equal to e.

One has to keep in mind that this approach is conducted in the framework of a linearized analysis. Therefore the results are valid only when the localization process is not too strongly developed. In the linearized approach the modes of instability can be analysed separately and the full solution is obtained by superposing the modes.

The parameter η, assumed constant in (24), is actually time-dependent since the roots of the algebraic equation (33), where the coefficients depend on the homogeneous solution, are time-dependent. Therefore, the linearized analysis is consistent only for perturbations which are growing much faster than the basic homogeneous solution, i.e. for a large enough value of e (see Molinari, 1985, and Fressengeas and Molinari, 1987, for more details).

The linearized stability analysis presented here is based on a Eulerian formulation. When a Lagrangian scheme is used, some small differences can be observed in the prediction of the rate of growth of the perturbation. These differences are negligible for fast growing perturbations.

4. ISOTROPIC MATERIAL UNDER ISOTHERMAL DEFORMATION

Concerning sheet metal forming, it is interesting to analyse the dependence of ε_x^c on the strain ratio ρ.

The simple case of an isotropic material under isothermal deformation, which can be compared with previous works, is first analysed.

To be consistent with the isothermal hypothesis, the thermomechanical coupling must be neglected in the energy equation (16); thus $\beta = 0$ and from (32) $B = 0$. One also has to set $\delta\theta^\circ = 0$, so that eqn (27) is identically satisfied. Formally it is equivalent to setting $\beta = 0$ and $k = 0$, i.e. $B = 0$ and $Q = 0$. Indeed, eqn (27) then implies $\dot{\eta} v \delta\theta^\circ/\theta^\circ = 0$ and the corresponding term disappears in (26). Then the characteristic equation (33) reduces to a third order equation which is the following quadratic equation multiplied by $\dot{\eta}$:

$$-\hat{\eta}^2 U^0_{2222}(mU^0_{2222}+T^0_{22})+\hat{\eta}\left[A^0_3(mU^0_{2222}+T^0_{22})-\frac{n}{\bar{\varepsilon}^0}U^2_{2222}+A^0_1A^0_2\right]+\frac{n}{\bar{\varepsilon}^0}A^0_3U^0_{2222}=0. \tag{39}$$

For an isotropic material, $F = G = H = N/3$ and the components of **T** and **U** in the frame (X, Y) depend only on ρ:

$$T^0_{xx}=\frac{2\sigma^0_{xx}-\sigma^0_{yy}}{2\bar{\sigma}^0}=\frac{\sqrt{3}}{2(1+\rho+\rho^2)^{1/2}}$$

$$T^0_{yy}=\frac{2\sigma^0_{yy}-\sigma^0_{xx}}{2\bar{\sigma}^0}=\frac{\sqrt{3}\rho}{2(1+\rho+\rho^2)^{1/2}}$$

$$T^0_{xy}=T^0_{yx}=0. \tag{40}$$

The components in the frame (x_1, x_2) axes are given by (11).

The value $n = 0.25$ is now assigned to the strain hardening parameter.

In Fig. 2, the roots (real) $\hat{\eta}^+$ and $\hat{\eta}^-$ of eqn (39) are represented versus the strain ε^0_x for $\rho = 0$ (plane strain case), for different values of the strain rate sensitivity m and for the orientation $\Psi = 0$. For a given m, $\hat{\eta}^+$ grows rapidly when the strain ε^0_x passes beyond the value $\varepsilon^0_x = n = 0.25$ corresponding to the maximum load Considère criterion. The growth is more significant when m is small. For $m = 0$, a singular behavior is observed; $\hat{\eta}^+$ tends to $+\infty$ when ε^0_x tends to n. For a given $e > 0$, the strain ε^c_x is increasing with m (stabilizing effect of the strain rate sensitivity). For $m = 0$, ε^c_x is independent on $e > 0$.

The dependence on the strain ratio ρ of the effective limit strain $\varepsilon^c_x = \inf_{\Psi} \varepsilon^c_x$ is illustrated in Fig. 3, where forming limit curves corresponding to different values of the effective instability parameter e are represented. The strain path varies from $\rho = -1/2$ (uniaxial tension) to $\rho = 1$ (equibiaxial stretching). The strain rate sensitivity is zero.

For $1 > \rho \geqslant 0$, the optimal orientation (which is $\Psi^c = \pi/2$ for $e = 0$) is equal to $\Psi^c = 0$ for $e > 0.3$ (Fig. 4a, b). For $\rho = 1$, the optimal orientation is undetermined (Fig. 4c). For

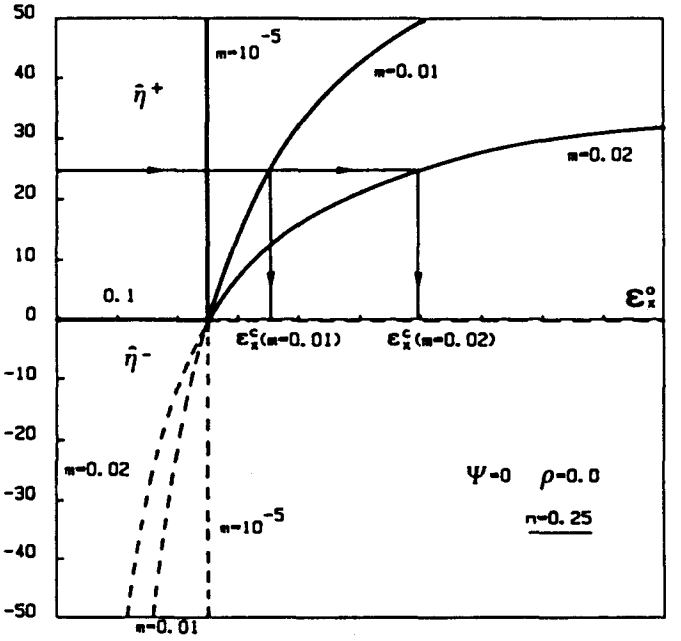

Fig. 2. For $\rho = 0$ (plane strain), $\Psi = 0$, $n = 0.25$, variations of the roots $\hat{\eta}^+$ and $\hat{\eta}^-$ in terms of the bulk homogeneous strain ε^0_x. The stabilizing effects of the strain rate sensitivity m are illustrated.

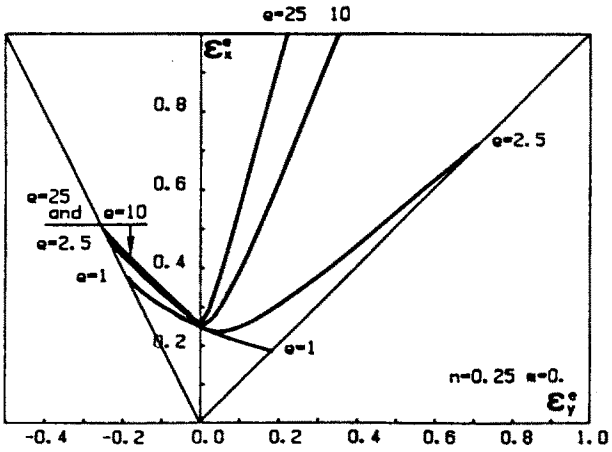

Fig. 3. Effective forming limit curves for $n = 0.25$; $m = 0$. The variations of ε_x^c are represented in terms of the strain ratio ρ, for different values of the effective instability parameter e.

$\rho < 0$, the optimal orientation Ψ^c is shown in Fig. 4d, e to depend strongly on the strain ratio ρ.

It is interesting to note that for large values $e = 10$, $\varepsilon_x^c(e = 10, \Psi^c) = \varepsilon_x^c(e = 0, \Psi^c)$ for $\rho \leqslant 0$ (Fig. 4d, e). This means that the mode of orientation Ψ^c, activated for the strain $\varepsilon_x^c(e = 0, \Psi^c)$, has an explosive growth since it attains instantaneously the rate of growth $e = 10$. This mode is dominant at the final stage of the instability process.

It is observed for increasing values of the effective instability parameter e, that the forming limit curves change their shape and tend to a limit for $\rho < 0$ (Fig. 3), when $m = 0$.

In Fig. 5, the growth of different modes in terms of the deformation is represented for $m = 0$. As noted previously, the optimal orientation Ψ^c minimizing the strain $\varepsilon_x^c(e, \Psi, \rho)$ depends generally on e (Fig. 5a). It is worthwhile noting that $\dot{\eta}^*$ is growing continuously for $\rho > 0$ (Fig. 5b), while it may present a singular behavior for $\rho < 0$ (Fig. 5a). For $\rho = -0.5$ and $\Psi = \Psi'' = 0.615$, $\dot{\eta}^*$ is suddenly growing to infinity when $\varepsilon_x^c = 2n = 0.5$.

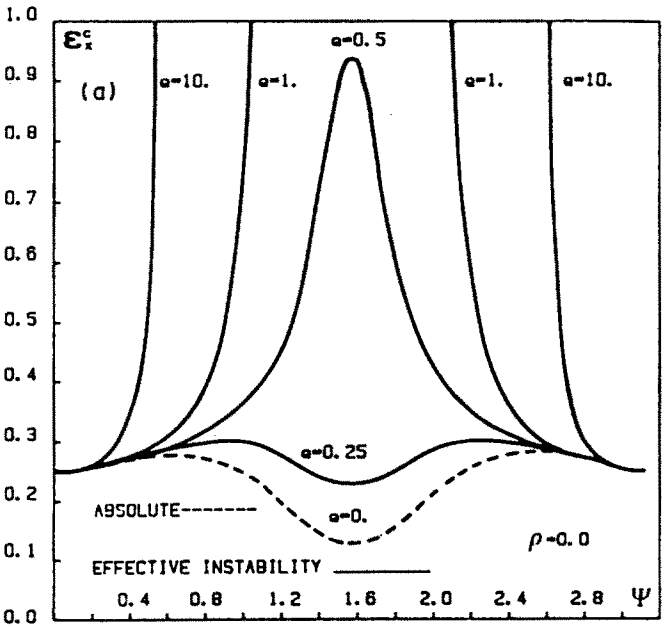

Fig. 4a.

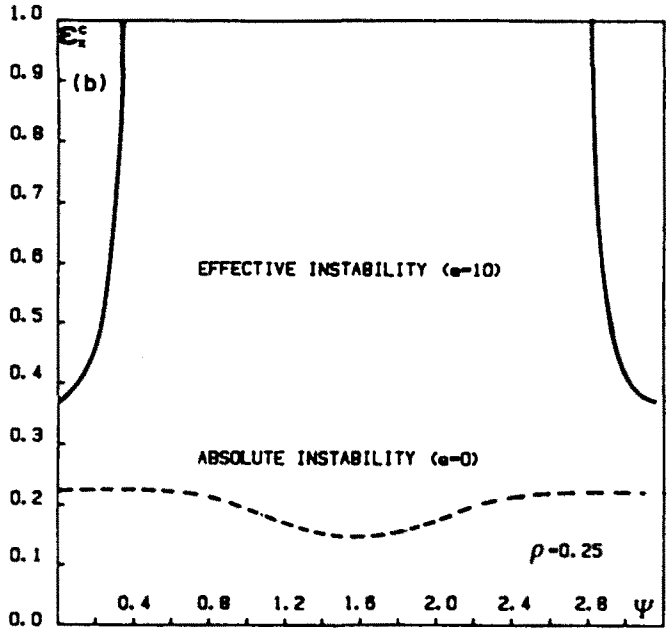
1.0
0.9
0.8
0.7
0.6
0.5
0.4
0.3
0.2
0.1
0.0
ε_1^c
(b)
EFFECTIVE INSTABILITY (α=10)
ABSOLUTE INSTABILITY (α=0)
ρ=0.25
0.4 0.8 1.2 1.6 2.0 2.4 2.8 Ψ

Fig. 4b.

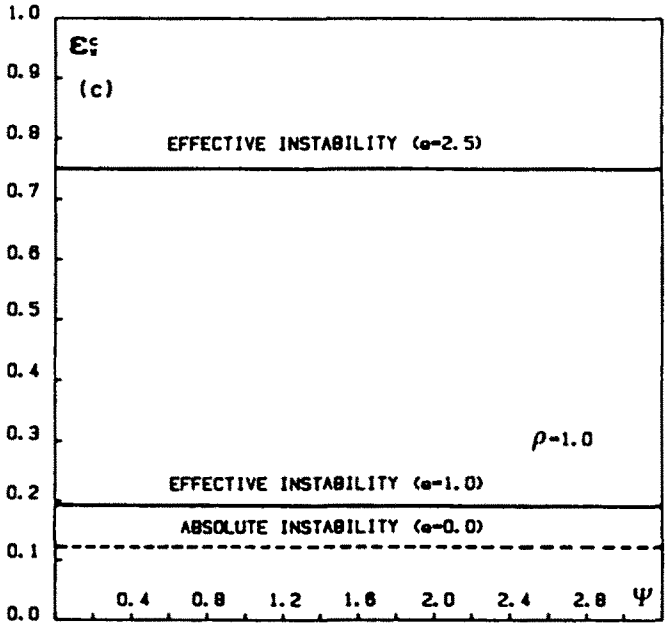
1.0
0.9
0.8
0.7
0.6
0.5
0.4
0.3
0.2
0.1
0.0
ε_1^c
(c)
EFFECTIVE INSTABILITY (α=2.5)
ρ=1.0
EFFECTIVE INSTABILITY (α=1.0)
ABSOLUTE INSTABILITY (α=0.0)
0.4 0.8 1.2 1.6 2.0 2.4 2.8 Ψ

Fig. 4c.

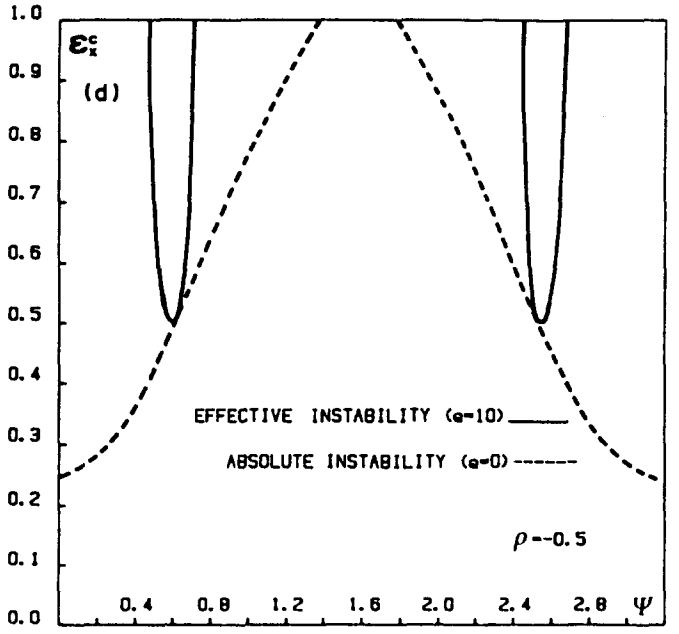

Fig. 4d.

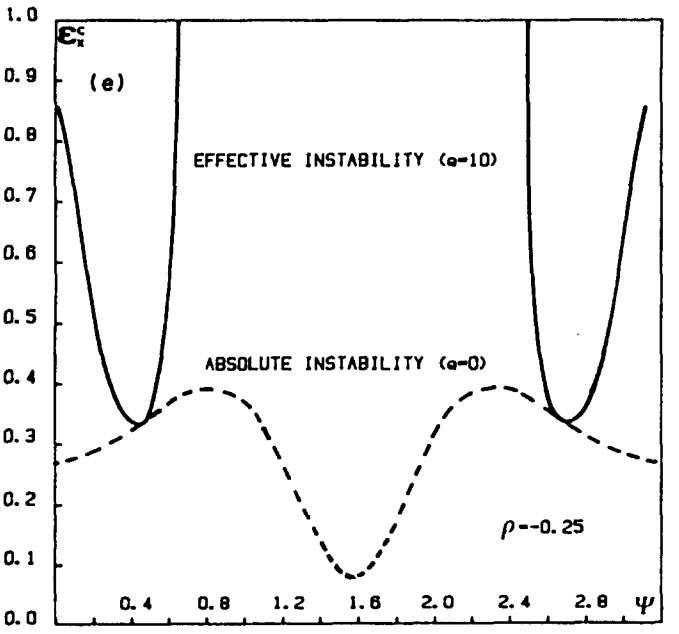

Fig. 4e.

Fig. 4. Dependence of ε_x^c on the orientation Ψ of the perturbation when $n = 0.25$ and $m = 0$. For values of the effective instability parameter $e > 0.3$, the optimal orientation is $\Psi^c = 0$ for $0 \leqslant \rho \leqslant 1$ (a, b). For $\rho = 1$, Ψ^c is undetermined (c). When $\rho < 0$, Ψ^c depends strongly on the strain ratio ρ.

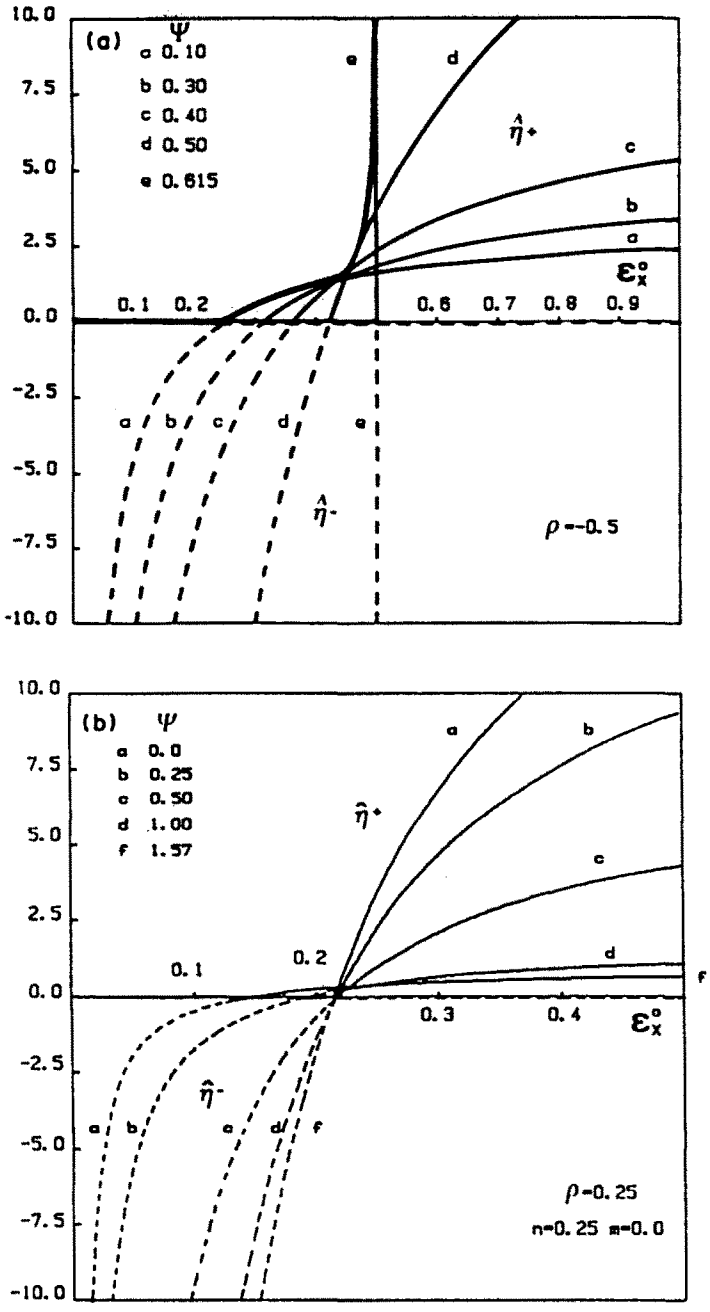

Fig. 5. Evolution of $\hat{\eta}^+$ and $\hat{\eta}^-$ in terms of the deformation ε_x^c, for different modes characterized by the orientation Ψ. The thick curve represents $\varepsilon_x^c(e,\rho) = \inf_{\Psi} \varepsilon_x^c(e,\Psi,\rho)$.

Therefore,

$$\varepsilon_x^c = \lim_{e\to\infty} \varepsilon_x^c(e, \Psi^H, \rho = -0.5) = 2n = 0.5. \tag{41}$$

Indeed, for $\rho < 0$, the forming limit curves are tending, when $e \to \infty$, to a limiting curve (Fig. 3) which will be proved to be the Hill curve (1952). More precisely, the following results are obtained. For $\rho \leqslant 0$

$$\lim_{e\to\infty} \Psi(e,\rho) = \Psi^H = \tan^{-1}\sqrt{-\rho} \tag{42}$$

$$\lim_{e\to\infty} \varepsilon_x^c(e,\rho) = \frac{n}{1+\rho}. \tag{43}$$

This means that, for a rate-independent material, the instability is fully developed (with an infinite rate of growth) when the strain ε_x^0 attains the limiting value given by (43). Then, the orientation of the dominant mode is given by (42). This is the orientation of the line of zero extension rate (Hill, 1952).

The proof of (42) and (43) relies on an asymptotic analysis. One seeks a particular mode of instability for the linearized problem, corresponding to the following asymptotic expansion with respect to m:

$$\dot{\eta} = \frac{1}{m}(\dot{\eta}_0 + m\dot{\eta}_1 + 0(m^2)). \tag{44}$$

The singular term $1/m$ has been included in order to restore the singular behavior of $\dot{\eta}^+$, for $\Psi = \Psi^H$, observed in Fig. 5a.

The subsitution of (44) into (39) leads to the following expression:

$$-\frac{1}{m} U^0_{2222} T^0_{22} \dot{\eta}_0 - \dot{\eta}_0 U^0_{2222} - \dot{\eta}_1 T^0_{22} U^0_{2222} + A^0_1 A^0_2 + A^0_3 T^0_{22} - \frac{n}{\bar{\varepsilon}^0} U^0_{2222} = 0. \tag{45}$$

It is readily checked that $\Psi = \Psi^H$ implies $T^0_{22} = 0$ and $U^0_{2222} = 1$. Then, the term $O(1/m)$ in (45) vanishes and the term $O(1)$ reads:

$$-\dot{\eta}_0 + \left(\frac{\sigma^0_{11}}{\bar{\sigma}^0} T^0_{11} + \frac{2\sigma^0_{12}}{\bar{\sigma}^0} T^0_{12}\right) T^0_{11} - \frac{n}{\bar{\varepsilon}^0} = 0. \tag{46}$$

For the mode $\Psi = \Psi^H$ we have:

$$\frac{\sigma^0_{11}}{\bar{\sigma}^0} = \frac{2(1+\rho)}{\sqrt{3(1+\rho+\rho^2)^{1/2}}}; \quad \frac{\sigma^0_{22}}{\bar{\sigma}^0} = \frac{1+\rho}{\sqrt{3(1+\rho+\rho^2)^{1/2}}}$$

$$\frac{\sigma^0_{12}}{\bar{\sigma}^0} = \frac{-\sqrt{-\rho}}{\sqrt{3(1+\rho+\rho^2)^{1/2}}}. \tag{47}$$

The onset of instability for that mode appears when $\dot{\eta}_0 = 0$. Using (46) and (47) this condition yields:

$$\varepsilon^0_x = \frac{n}{1+\rho}. \tag{48}$$

Therefore, the mode $\Psi = \Psi^H$ coincides with Hill's solution (1952) asymptotically when $m \to 0$. It is worthwhile noting that due to the $1/m$ singularity, the growth rate of that mode ($\dot{\eta} = \dot{\eta}_0/m$) is very fast when $m \to 0$. Thus, for $m = 0$ and for large values $e > 0$, the dominant mode is associated to $\Psi = \Psi^H$. The effective limit strain is then given by (48). Thus for a rate-independent material $\rho < 0$, the effective stability analysis leads to the same results as the Hill localization analysis (1952).

In biaxial stretching ($\rho > 0$), the optimal angle is $\Psi^c = 0$ if e is large enough. In opposition to the paths $\rho \leqslant 0$, $\dot{\eta}^+$ does not present any singular behavior (Fig. 5b). Therefore, when e increases, the growth of ε^c_x is unbounded (Figs 3 and 5b). The fact that, for $e = 10$, no effective instability appears in equibiaxial stretching (Fig. 3) can be related to previous works which have shown that a band mode bifurcation is not possible for strain path $\rho > 0$ and for a rigid plastic material obeying a flow law associated to a smooth yield surface (no vertex) (Stören and Rice, 1975; Hutchinson and Neale, 1978). Our analysis shows, however, that band mode perturbations may grow (in agreement with the M.K. analysis) but with a low rate of growth. The solution is unique (no bifurcation) but unstable.

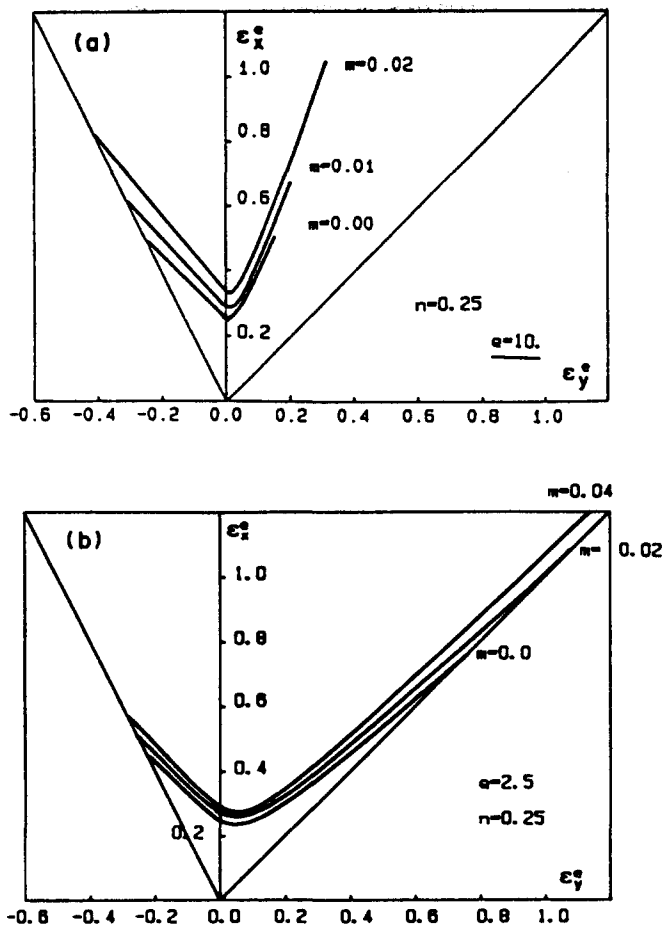

Fig. 6. Stabilizing effects of the strain rate sensitivity m on the effective forming limit curves $e = 10$ and $e = 2.5$.

The stabilizing effect of the strain rate sensitivity m is illustrated in Fig. 6. The forming limit curves are associated to the values $e = 2.5$ and $e = 10$ of the effective instability parameter.

Figure 7 illustrates the variation with the orientation Ψ of the critical strain $\varepsilon_x^c(e, \Psi, \rho = -0.5)$ in uniaxial tension (for $e = 0$ and $e = 10$). The optimal orientation is shown to be independent of the strain rate sensitivity m, while the level of ε_x^c is strongly affected by m for $e > 0$. It is worthwhile noting that the strain ε_x^u corresponding to the onset of instability is not affected by the strain rate sensitivity. It is recalled that for $e = 10$, the orientation Ψ^c corresponds to the zero extension line.

The growth of $\dot{\eta}^+$ is represented in Fig. 8, for $\rho = -0.5$ and for the orientation $\Psi = \tan^{-1}\sqrt{-\rho} = 0.615$ which is optimal (and equal to Hill's orientation) when e is large enough. The singular behavior of $\dot{\eta}^+$ existing for $m = 0$, is smoothed when the strain rate sensitivity is different from zero.

5. THERMAL EFFECTS

The ductility of materials during forming processes can be significantly influenced by thermal softening. The decrease of the yield stress for increasing temperatures is a crucial factor affecting the plastic flow localization. A thermoviscoplastic instability results from the heat generated by plastic deformation that can be concentrated in narrow regions (Tresca, 1878; Zener and Hollomon, 1944).

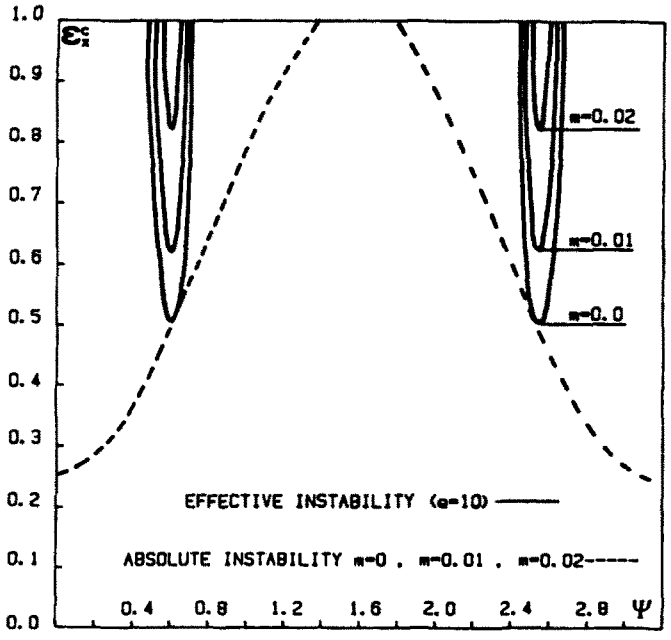

Fig. 7. Dependence of ε_1^c in terms of Ψ for $\rho = -0.5$, for $e = 0$ and $e = 10$, and different values of the strain rate sensitivity m ($n = 0.25$). It appears that the optimal orientation Ψ^c is independent of m. The value of the effective instability strain $\varepsilon_1^c = \inf_{\Psi} \varepsilon_1^c$ is strongly affected by m for $e = 10$, but not for $e = 0$. Thus, the critical strain corresponding to the onset of instability does not depend on m.

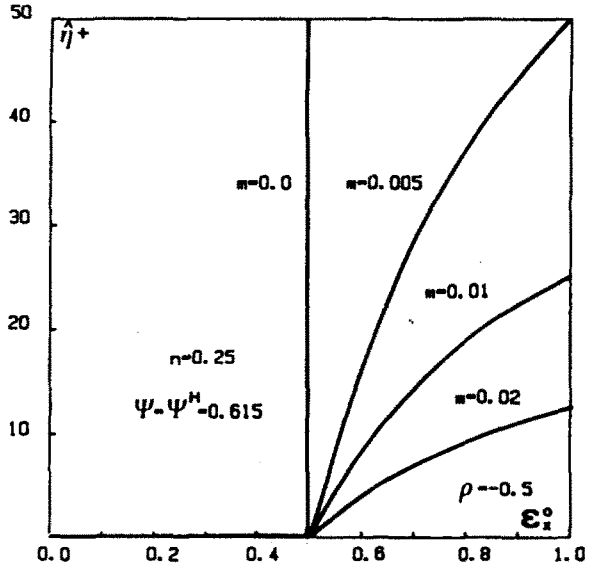

Fig. 8. Evolution of the growth rate $\hat{\eta}^+$ of the perturbation associated with the optimal orientation $\Psi = \Psi^H = 0.615$ for $\rho = -0.5$. When $m = 0$ this perturbation presents an explosive growth for the strain $\varepsilon_1 = n(1+\rho) = 2n$ given by Hill's analysis. This singular behavior is smoothed by the strain rate sensitivity.

For materials presenting a low thermal conductivity (e.g. polymers, stainless steel) or for high strain rate processes, this localized heating is possible since the characteristic time of thermal conduction (associated to the defect under consideration) is large compared to the duration of the localization process.

Experimental evidence of the role of thermoplastic instabilities has been presented, e.g. by Ferron (1981) for simple tension test at room temperature, Dodd and Atkins (1983) for

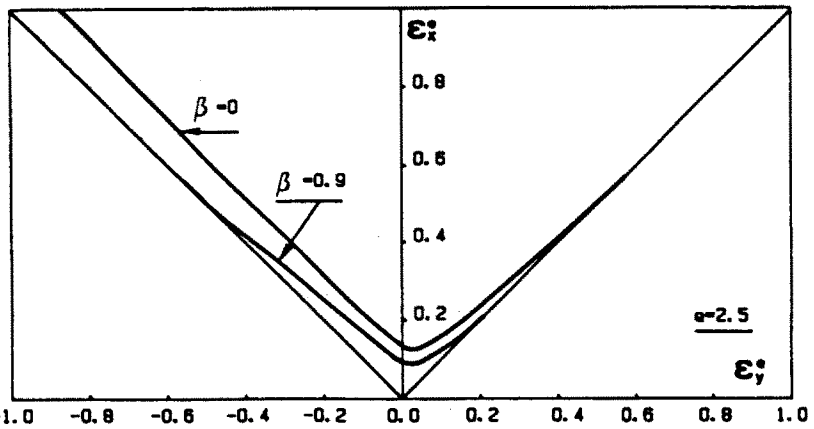

Fig. 9. The heat conductivity is zero. The forming limit curve $\beta = 0.9$ illustrates the destabilizing effect of the thermal softening (which is zero for the isothermal curve, $\beta = 0$). For the simple shearing path $\rho = 1$, no instability occurs when $\beta = 0$. An adiabatic shear band appears for $\beta = 0.9$ ($\mu = 1.41 \times 10^{10}$ SI, $n = 0.12$, $m = 0.0133$, $\nu = -0.51$).

sheet metal forming, and in review papers by Rogers (1979) and Bedford *et al.* (1974) for shear instabilities.

A theoretical analysis of thermoplastic instabilities in sheet metal forming has been presented by Ferron and Mliha-Touati (1985) in the framework of a linearized Lagrangian defect analysis and by Dudzinski and Molinari (1985) for a kinematic hardening and temperature-sensitive material.

Here we present a discussion of the influence of thermal softening on the plastic flow instability. Necking and shear banding in biaxially loaded ductile metal sheets are considered. Only the formation of shear bands parallel to the plane of the sheet is addressed here. The occurrence of shear bands in the cross-section of the neck, at the final stage of the process, just before rupture, is not discussed.

The material is isotropic and rigid plastic. We assume that the strain rates are not too high so that inertia effects are negligible. The calculations are carried out with the following material parameters [see eqn (7)]:

$$\mu = 1.41 \times 10^{10}\,\text{SI}$$

$$n = 0.12$$

$$m = 0.0133$$

$$\nu = -0.51.$$

The heat capacity is:

$$C = 3.6 \times 10^6\ \text{J/m}^3 \cdot {}^\circ\text{K}.$$

These parameters are representative of an HRS steel (Clifton *et al.*, 1984).

The homogeneous temperature is given by:

$$\theta^\circ = \left[\frac{\beta\mu(\dot{\bar{\varepsilon}}^\circ)^m}{c}\,\frac{1-\nu}{1+n}\,\bar{\varepsilon}^{\circ(1+n)} + \theta^{\circ}(0)^{(1-\nu)}\right]^{1/(1-\nu)} \tag{49}$$

where $\theta^\circ(0)$ is the initial homogeneous temperature. This results from the integration of the energy equation (16), where all terms in the second member disappear except $\beta\bar{\sigma}\dot{\bar{\varepsilon}}$. The expression (7) of $\bar{\sigma}$ has been used.

The growth rate of the perturbation is governed by the roots of the cubic equation (33). The effect of thermal softening is illustrated in Fig. 9, where the heat conductivity is

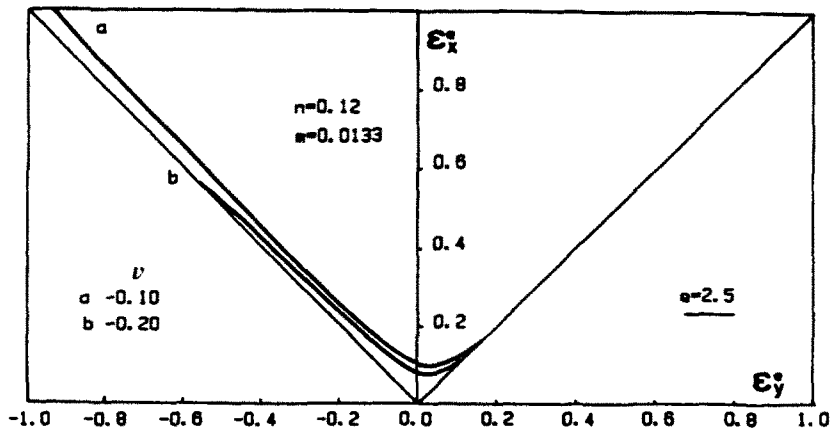

Fig. 10. Instability for $\rho = -1$ can occur only if $\nu+n < 0$.

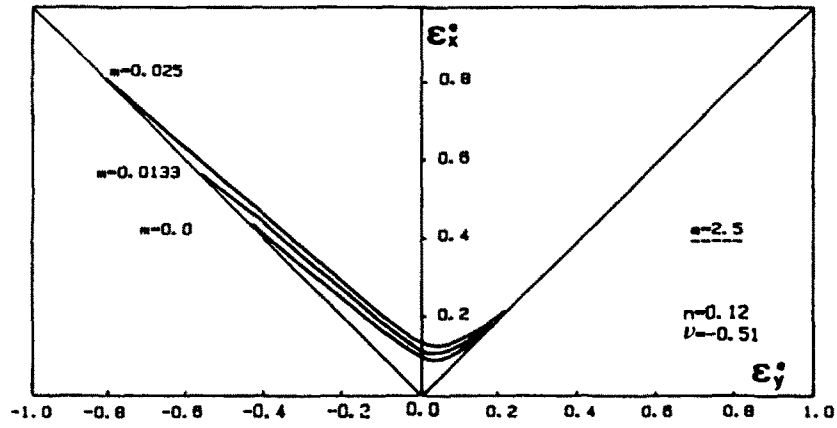

Fig. 11. The strain rate sensitivity is strongly stabilizing for paths close to $\rho = -1$.

assumed to be zero. The limit curves are calculated for $e = 2.5$. The curve $\beta = 0$ corresponds to an isothermal process: the thermomechanical coupling in the energy equation (16) is cancelled, thus the temperature keeps its initial value $\theta^*(0)$. The second curve, corresponding to $\beta = 0.9$, takes account of the thermomechanical coupling. A global decrease of the critical strains, due to the thermal softening that promotes instability, is observed. Moreover, for the path $\rho = -1$ corresponding to simple shearing, an instability is depicted, while it is not for $\beta = 0$. This instability results from the following well known autocatalytic process: at some place a perturbation of the temperature field generates a local material softening and thus a local increase of the strain rates, which in turn generates more heat production. This thermoviscoplastic instability sometimes degenerates in a localized shear band (so called adiabatic shear band), as is the case here for $\rho = -1$.

For paths $-1 < \rho < 0$ the instability mode results from a combination of shear and necking modes.

Thermal softening is a necessary but not a sufficient condition for thermoviscoplastic shear instability. Simple shearing of a thermoviscoplastic material becomes unstable when strain hardening is overcome by thermal softening (Zener and Hollomon, 1944). For the power law (7) shear instability will occur (but not necessarily localization, see Molinari, 1985; Fressengeas and Molinari, 1987), if and only if $\nu+n < 0$ (ν is negative for a thermal softening material). This is illustrated in Fig. 10, where it appears that the ducility is infinite for $\rho = -1$ when $\nu+n > 0$.

Strain rate sensitivity is a very stabilizing factor for paths close to $\rho = -1$ (Fig. 11). This is in agreement with theoretical analysis of simple shear instability (Molinari and Clifton, 1987).

Heat conduction refrains the temperature localization. Its stabilizing effect is more pronounced for paths close to $\rho = -1$ (Fig. 12). When the non-dimensional heat conductivity Q is equal to zero, the effects of heat conduction are negligible (low heat conducting material, or fast process). When Q is large the problem is isothermal and shear localization for $\rho = -1$ is hindered (Fig. 12).

6. ANISOTROPY

The influence of the material anisotropy is analysed now. Only the case of orthotropic symmetry will be considered. This plastic anisotropy can be characterized by the ratio of the transverse to the through-thickness strain measured in uniaxial tension for three directions (R_0, R_{45}, R_{90}) where 0°, 45° and 90° represent the angles of the tensile axe with respect to the rolling direction (see Appendix A). Barata de Rocha and Jalinier (1984) have analysed the effect of an initial orthotropic anisotropy, combined with isotropic hardening, on the formability of stretched sheets. Using the defect theory of Marciniak and Kuszynski (1967), they calculated the forming limit curves at localization.

A quantitative comparison between the results of the M.K. theory and those of the effective instability analysis is difficult to establish. Indeed, the results of the M.K. theory depend on the amplitude of the initial defect, while the results of the effective instability analysis depend on the intensity of the parameter e. Nevertheless, it is expected that for an appropriate value of e, the prediction of the perturbation analysis should present the same trends as that of the M.K. localization analysis.

A material exhibiting normal anisotropy ($R = R_0 = R_{45} = R_{90}$) is first considered. The higher the value of the anisotropy parameter R, the sharper is the curvature of Hill's yield locus in the region of symmetric biaxial loading (Fig. 13).

The exponent 'j' characterizing the growth rate of the perturbation is a root of the algebraic equation (33). The forming limit curves are calculated for $e = 2.5$ and $e = 10$ (Fig. 14). The stress ratio α varies from uniaxial tension ($\alpha = 0$) to equibiaxial tension ($\alpha = 1$). As shown in Appendix A, the strain path ρ corresponding to uniaxial tension ($\alpha = 0$) is given by:

$$\rho = \frac{-R}{1+R}. \tag{50}$$

For $\rho \geqslant 0$, high R-values allow the condition for instability at an earlier stage of the

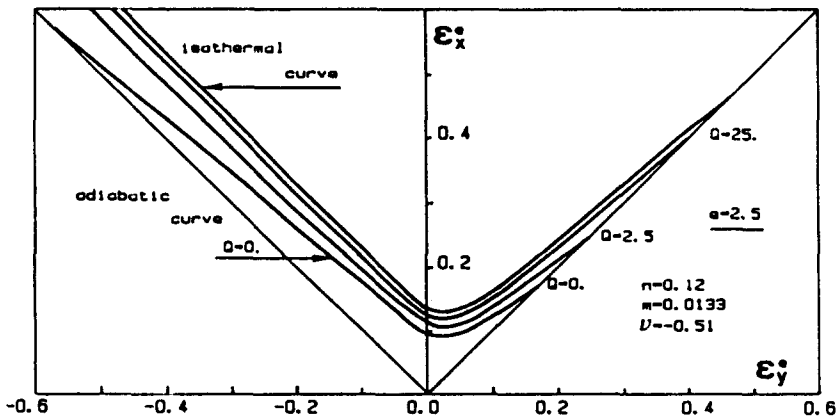

Fig. 12. Stabilizing effect of heat conduction.

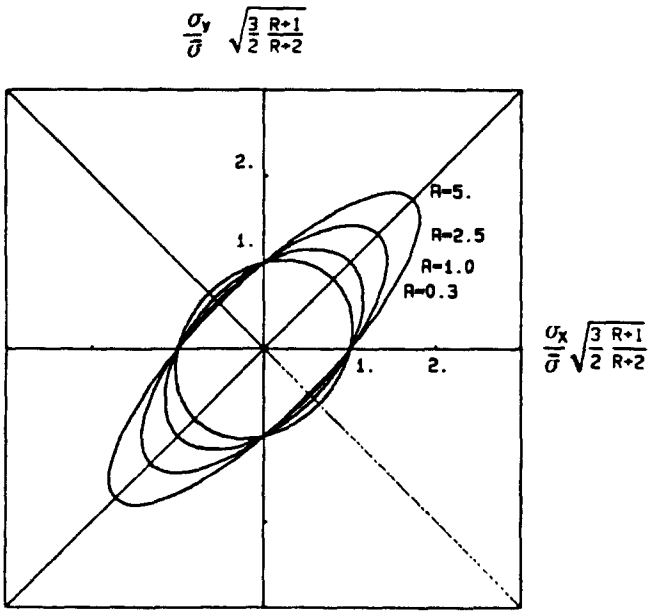

Fig. 13. For normal anisotropy, the curvature of Hill's yield surface at the equibiaxial loading point increases with the anisotropic parameter R.

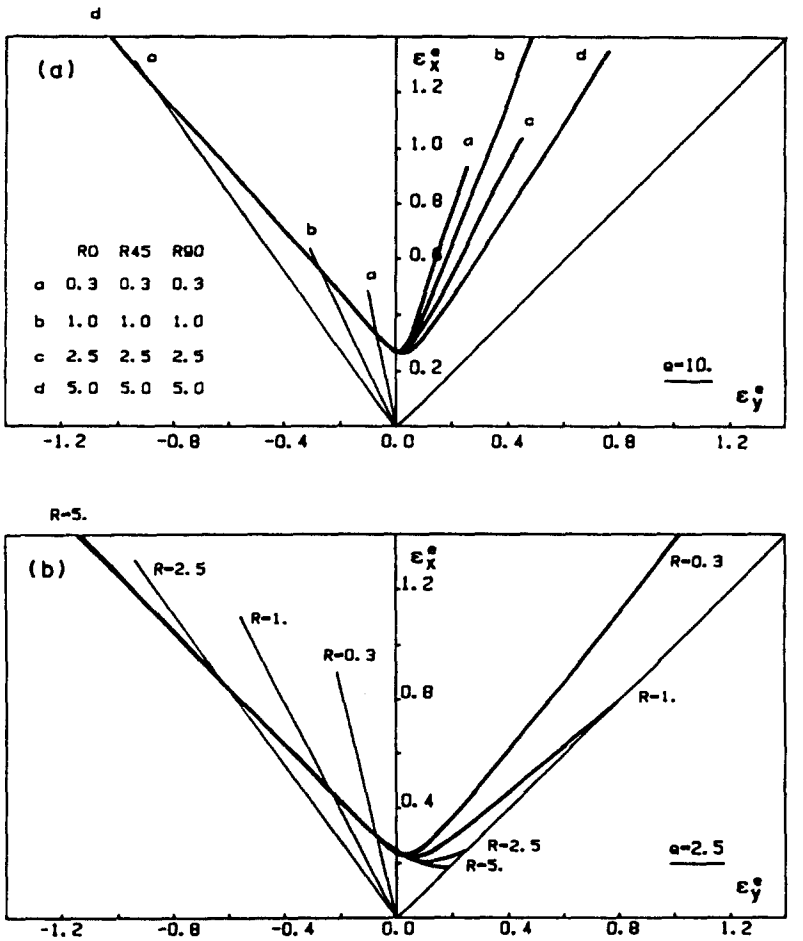

Fig. 14. Increasing values of the parameter R, characterizing the normal anisotropy, are destabilizing for the strain paths $\rho > 0$ ($n = 0.22$ and $m = 0.012$).

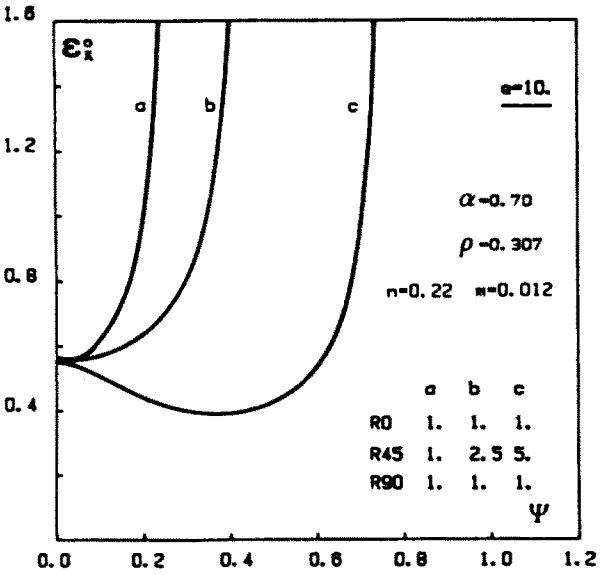

Fig. 15. Dependence of ε_x^c with respect to Ψ for the stress path $\alpha = 0.7$ and $e = 10$. When $R_{45} = 5$. the optimal orientation Ψ^c is different from zero.

deformation and result in reduced limit strains (Fig. 14). As demonstrated by many authors, e.g. Tvergaard (1978), and Ferron and Mliha-Touati (1985), this is an effect of the yield surface curvature. For increasing R, the curvature is larger at the equibiaxial loading point (Fig. 13). Then, the plastic flow is less stable for $\rho > 0$.

It can be noted in Fig. 14 that the growth of the instability is very slow for equibiaxial loading, even for $R = 5$. When $e = 10$, $\rho = 1$, the limit strain ε_x^c is infinite while it is finite when $e = 2.5$. For this straining path, the instability process does not really lead to a fast growing localized necking band, as is usual for a flow law associated to a smooth yield surface.

A complete analysis of the effect of R_0, R_{45} and R_{90} can be easily done with the proposed perturbation method and leads to the same qualitative results as those obtained by Barata de Rocha and Jalinier (1984) with an M.K. analysis.

Another illustration is given by the effect of R_{45}. In Fig. 15, ε_x^c is represented versus the orientation Ψ for $e = 10$ and $\rho = 0.307$, and for different values of R_{45}. When $R_{45} = 5$, the effective optimal orientation Ψ^c is different from zero, while for an isotropic medium Ψ^c is zero. This effect of anisotropy has been noted by Barata da Rocha and Jalinier (1984).

7. DEFORMATION THEORY

In order to bring out in a more explicit manner the effect of the local shape of the yield surface on the forming limit curves in the positive ρ range, we now focus on results obtained from the deformation theory of plasticity. Stören and Rice (1975) demonstrated that the deformation theory of plasticity is equivalent to a flow theory which permits the development of a pointed vertex on the yield surface. These authors incorporated the deformation theory into a classical bifurcation analysis for rate-insensitive materials. We consider here a rate-sensitive anisotropic deformation theory.

The material is incompressible, rigid-plastic and transversely isotropic (normal anisotropy). The constitutive law used here is associated with the plane stress Hill yield function [eqn (A6)]

$$\bar{\sigma} = \sqrt{\frac{3}{2}}\sqrt{\frac{R+1}{R+2}}\left[\sigma_1^2+\sigma_2^2-\frac{2R}{1+R}\sigma_1\sigma_2\right]^{1/2} \tag{51}$$

where σ_1 and σ_2 are the principals in plane stresses. The 1-axis here is identical to the x-axis, since the orientation of the perturbation is taken to be $\Psi = 0$.

An appropriate measure of strain is the logarithmic strain tensor, whose principal values are given by:

$$\varepsilon_i = \ln \lambda_i \tag{52}$$

where $(\lambda_1, \lambda_2, \lambda_3)$ are the three principal stretches relative to the reference configuration. The incompressibility condition becomes:

$$\lambda_1 \lambda_2 \lambda_3 = 1 \tag{53}$$

or

$$\varepsilon_1 + \varepsilon_2 + \varepsilon_3 = 0. \tag{54}$$

The constitutive law is formulated as follows:

$$\begin{aligned} \varepsilon_{11} &= T_{11}\bar{\varepsilon} \\ \varepsilon_{22} &= T_{22}\bar{\varepsilon} \end{aligned} \tag{55}$$

with

$$\begin{aligned} T_{11} &= \frac{\partial \bar{\sigma}}{\partial \sigma_1} = \frac{3}{2}\frac{R+1}{R+2}\left(2\sigma_1 - \frac{2R}{R+1}\sigma_2\right)\Big/ 2\bar{\sigma} \\ T_{22} &= \frac{\partial \bar{\sigma}}{\partial \sigma_2} = \frac{3}{2}\frac{R+1}{R+2}\left(2\sigma_2 - \frac{2R}{R+1}\sigma_1\right)\Big/ 2\bar{\sigma}. \end{aligned} \tag{56}$$

The viscoplastic response of the material is governed by (55) and the hardening law (7)

$$\bar{\sigma} = \mu \bar{\varepsilon}^m \dot{\bar{\varepsilon}}^m. \tag{57}$$

We restrict the stability analysis to biaxial stretching ($\rho > 0$). Perturbations of orientation $\Psi = 0$ only are considered. This is justified for normal anisotropy but not for a general anisotropy (Barata da Rocha and Jalinier, 1984). The compatibility conditions (12) and the equilibrium equations (13) are written in the simple form:

$$\frac{1}{2}\left(\frac{\partial^2 \dot{\varepsilon}_1}{\partial x_2^2} + \frac{\partial^2 \dot{\varepsilon}_2}{\partial x_1^2}\right) = 0 \tag{58}$$

$$\frac{\partial (h\sigma_1)}{\partial x_1} = 0; \quad \frac{\partial (h\sigma_2)}{\partial x_2} = 0. \tag{59}$$

A perturbation analysis of eqns (51), (54), (55), (57), (58) and (59) gives the following linear equation with respect to $\dot{\eta}$ [the identity $(U^0_{1111}U^0_{2222} - U^0_{1122}U^0_{2211}) = 0$ is used]:

$$m\bar{\varepsilon}^0 U^3_{2222}\dot{\eta} + (T^3_{22} + nU^0_{2222})U^0_{2222} - \bar{\varepsilon}^0 \frac{\sigma_1^3}{\bar{\sigma}^3}(T^0_{11}U^0_{2222} - T^0_{22}U^0_{1122})^2 = 0 \tag{60}$$

where T^0_{11} and T^0_{22} are given by (56) and where:

$$\begin{aligned} U^1_{1111} &= \bar{\sigma}^1\left(\frac{\partial T_{11}}{\partial \sigma_{11}}\right)^1 = \frac{3}{2}\frac{R+1}{R+2} - T^3_{11} \\ U^1_{2222} &= \bar{\sigma}^1\left(\frac{\partial T_{22}}{\partial \sigma_{22}}\right)^1 = \frac{3}{2}\frac{R+1}{R+2} - T^3_{22} \\ U^0_{1122} &= \bar{\sigma}^1\left(\frac{\partial T_{11}}{\partial \sigma_{22}}\right)^0 = \bar{\sigma}^1\left(\frac{\partial T_{22}}{\partial \sigma_{11}}\right)^0 = -\frac{3}{2}\frac{R}{R+2} - T^0_{11}T^0_{22}. \end{aligned} \tag{61}$$

From (60) it results that an instability of intensity e occurs for the following critical strain:

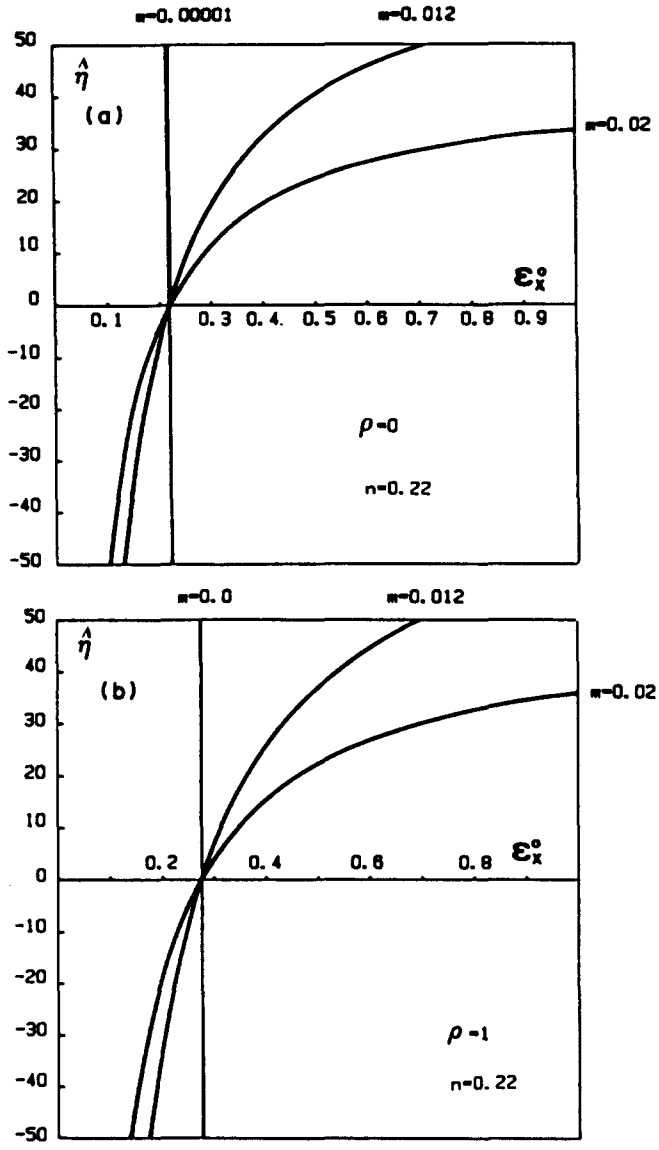

Fig. 16. Evolution of the growth rate $\dot{\eta}$ in terms of the deformation ε_x^c, for different values of the strain rate sensitivity m and for $\rho = 0$ (16a) and $\rho = 1$ (16b). It can be noted that for $\rho = 1$, $\dot{\eta}$ presents a singular behavior when m tends to zero, which is not the case for the flow theory (Fig. 5b). This is a vertex effect.

$$\varepsilon_x^c(e,\rho) = \sqrt{\frac{3}{2}}\sqrt{\frac{(1+2R)}{(2+R)(1+R)}}\frac{\bar{\varepsilon}^\circ}{\left(1+\frac{2R}{1+R}\rho+\rho^2\right)^{1/2}} \tag{62}$$

with

$$\bar{\varepsilon}^\circ = \frac{(T^\circ_{22}+nU^\circ_{2222})U^\circ_{2222}}{-mU^{\circ 2}_{2222}e+\frac{\sigma_1^\circ}{\bar{\sigma}^\circ}(T^\circ_{11}U^\circ_{2222}-T^\circ_{22}U^\circ_{1122})^2} \tag{63}$$

The onset of instability starts for the strain $\varepsilon_x^c(e=0,\rho)$. For a vanishing strain rate sensitivity the growth of this instability is explosive. This is due to the singular behavior of $\dot{\eta}$ illustrated in Fig. 16. For an isotropic rate-independent material ($n = 0.22, m = 0, R = 1$), the relation (62) brings out the same results as those found by Stören and Rice (1975).

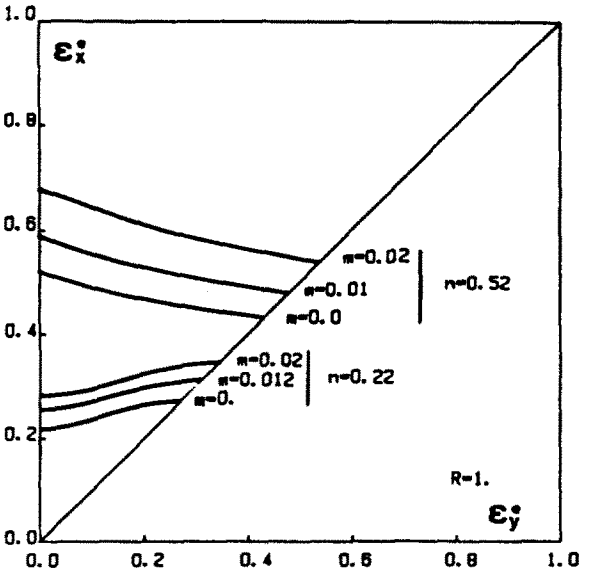

Fig. 17. Effective forming limit curves ($e = 10$) for a low hardening material ($n = 0.22$) and a high hardening material ($n = 0.52$). An isotropic deformation theory is considered ($R = 1$).

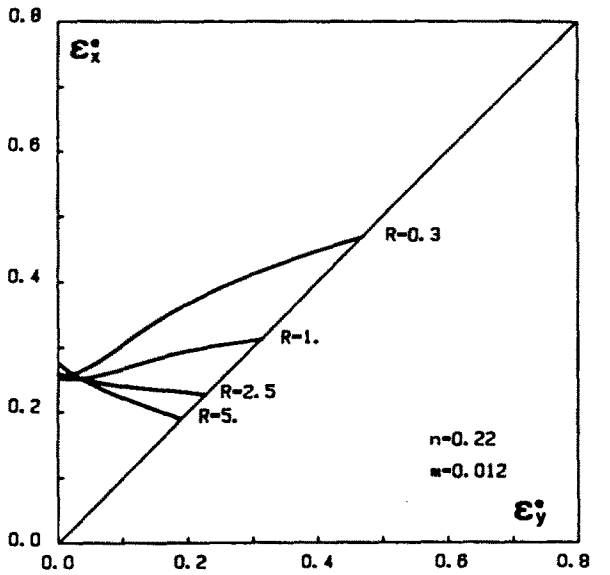

Fig. 18. Deformation theory and effects of the anisotropic parameter R ($e = 10$).

In Fig. 17 are represented the forming limit curves for two values of the strain hardening parameter ($n = 0.22$ and $n = 0.52$), for various values of the strain rate sensitivity coefficient m, and for the effective instability parameter $e = 10$. The well known destabilizing effect of the vertex for the path $\rho = 1$ is clear when the limit curves of Fig. 17 are compared with those of Fig. 6.

It is worthwhile to note that although the vertex is rounded by the rate sensitivity effect, this does not prevent a fast development of the instability for $\rho = 1$. Basically, the forming limit curves are translated up by the stabilizing effect of the strain rate sensitivity, which curiously enough is not stronger for the path $\rho = 1$.

The combined effects of the initial anisotropy characterized by the R-value and of the vertex involved by the deformation theory are illustrated by Fig. 18 for $e = 10$. These results are in agreement with those obtained by Neale and Chater (1980).

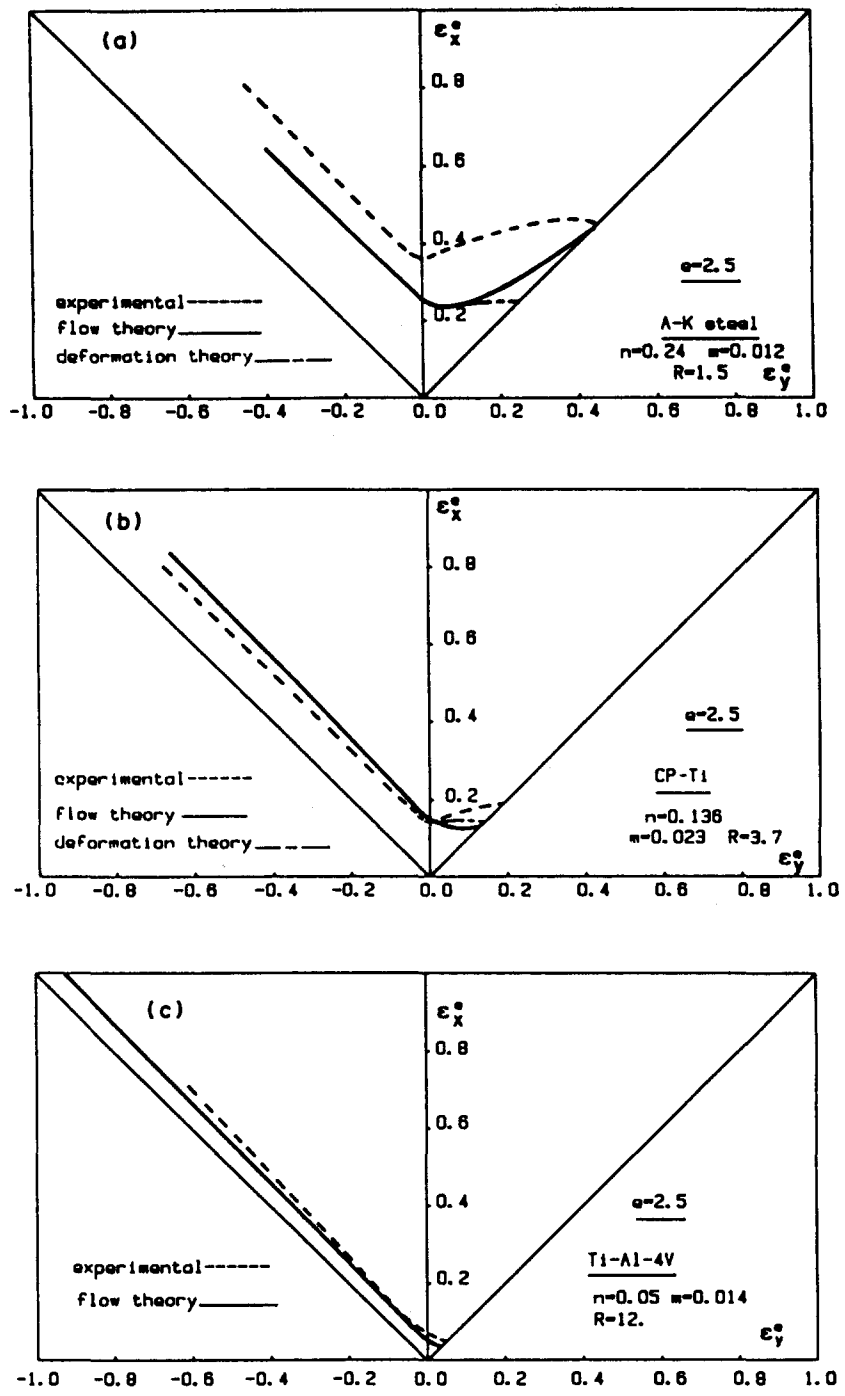

Fig. 19. Results of the deformation theory (restricted to $\rho > 0$) and of the flow theory, for $e = 2.5$, are compared with experiments. (a) For an A.K. steel; (b, c) for CP-Ti and Ti-Al-4V. From Chan (1985).

Finally, the results of the deformation theory (restricted to $\rho \geqslant 0$) and of the flow theory are compared with experiments in Fig. 19. As discussed earlier, the results of the instability analysis are very sensitive to the value of the effective instability parameter for $\rho > 0$, in the case of flow theory. For $e = 2.5$ the global shape and level of forming limit curves calculated with the flow theory is shown to be comparable to the experimental curves except for the A.K. steel (Fig. 19a). For that value of e, the growth rate of the faster modes is 2.5 times larger than the growth rate of the homogeneous strains.

8. CONCLUSION

The effective instability approach has been proven to be a useful tool in the analysis of sheet metal ductility. The onset of instability appears to be of little significance if the growth of the unstable modes is very slow.

The intensity e of the instability process is characterized in the following way: e is, at a given stage of the deformation, the rate of growth of the fastest unstable mode in the linearized perturbation analysis. The onset of instability corresponds to $e = 0$, but the instability is effective only for a significantly large value of e. It is emphasized that, as discussed at the end of Section 3, the linearized analysis presented here is completely justified for large enough values of e.

The effective instability analysis gives basically the same trends as the M.K. defect analysis. The dependence of the limit strains on the value of the instability intensity parameter e presents the same tendencies as the dependence of the limit strains on the amplitude of the initial defect in the M.K. analysis. However, it must be noted that the M.K. analysis can be viewed as a post-bifurcation analysis, while the effective instability analysis is basically a linearized approach.

The effective instability analysis works for quite general material behavior (including heat conduction and dynamic problems) and leads to simple analytical results where the effects of the physical parameters are easily discussed.

Moreover, the match with previous bifurcation analysis for rate-independent behavior (Hill, 1952; Stören and Rice, 1975; Hutchinson and Neale, 1978) appears clearly when $e \to \infty$. The results of these authors have been extended to rate-dependent problems and more complex material behavior.

REFERENCES

Bai, Y. L. (1982). *J. Mech. Phys. Solids* **30**, 196.
Barata da Rocha, A. and Jalinier, J. M. (1984). *Trans. ISIJ* **24**, 132.
Bedford, A. J., Wingrove, A. L. and Thompson, K. R. L. (1974). *Aust. Inst. Metals* **19**, 61.
Canova, G. R., Kocks, U. F., Fressengeas, C., Dudzinski, D., Lequeu, Ph. and Sornberger, G. (1987). *ICOTOM* **8**, Santa Fe, NM, U.S.A.
Chan, K. S. (1985). *Metall. Trans.* **16A**, April, 639.
Clifton, R. (1978). Report to the NRC Committee on material response to ultrasonic loading rates.
Clifton, R. J., Duffy, J., Hartley, K. W. and Shawki, T. G. (1984). *Scripta Metall.* **18**, 443.
Dodd, B. and Atkins, A. G. (1983). *Acta Metall.* **31**, 9.
Dudzinski, D. and Molinari, A. (1985). *Proc. Symp. Plastic Instability*, Considère Memorial, Paris France, Presses des Ponts et Chaussées, p. 25.
Dudzinski, D. and Molinari, A. (1988). *C.R. Acad. Sci. Paris* **307**, sér. II, 1315.
Ferron, G. (1981). *Mater. Sci. Engng* **49**, 241.
Ferron, G. and Mliha-Touati, M. (1985). *Int. J. Mech. Sci.* **27**(3), 121.
Fressengeas, C. and Molinari, A. (1985). *Acta Metall.* **33**(3), 387.
Fressengeas, C. and Molinari, A. (1987). *J. Mech. Phys. Solids* **35**(2), 185.
Hill, R. (1950). *The Mathematical Theory of Plasticity*. Oxford University Press.
Hill, R. (1952). *J. Mech. Phys. Solids* **1**, 19.
Hutchinson, J. W. and Neale, K. W. (1978). *Mechanics of Sheet Metal Forming*. Plenum Press, New York.
Marciniak, Z. and Kuczynski, K. (1967). *Int. J. Mech. Sci.* **9**, 609.
Molinari, A. (1985). *J. Méc. Théor. Appl.* **4**(5), 659.
Molinari, A. and Clifton, R. J. (1987). *J. Appl. Mech.* **54**, 806.
Neale, K. W. and Chater, E. (1980). *Int. J. Mech. Sci.* **22**, 563.
Rogers, H. C. (1979). *Ann. Rev. Mater. Sci.* **9**, 283.
Stören, S. and Rice, J. R. (1975). *J. Mech. Phys. Solids* **23**, 421.
Tresca, H. (1878). *Proc. Inst. Mech. Engrs* **30**, 301.
Tvergaard, V. (1978). *Int. J. Mech. Sci.* **20**, 651.
Zener, C. and Hollomon, J. H. (1944). *J. Appl. Phys.* **15**, 22.

APPENDIX A

In uniaxial tension, the ratio of the transverse to the through-thickness strain is, for an orthotropic material (Hill, 1950):

$$R_\phi = \frac{H + (2N - F - G - 4H)\sin^2\phi\cos^2\phi}{F\sin^2\phi + G\cos^2\phi} \tag{A1}$$

where ϕ is the angle of the tension axis with the rolling direction of the sheet (x-direction). The R-values at 0°, 45° and 90° are

$$R_0 = H/G$$

$$R_{45} = \frac{2N-(F+G)}{2(F+G)} \quad \text{or} \quad \frac{N}{G} = (R_{45}+\tfrac{1}{2})\left(1+\frac{R_0}{R_{90}}\right). \tag{A2}$$

The principal axis of anisotropy (x, y) coincides with the principal axes of strain rate and stresses (X, Y) as long as the deformation is uniform. The principal values of strain rates are D_{xx} and D_{yy}, the principal values of stresses are $\sigma_x = \sigma_{xx}$ and $\sigma_y = \sigma_{yy}$. The effective stress (3) and the effective strain rate (6) can be expressed in terms of these principal values:

$$\bar{\sigma} = \sqrt{\frac{3}{2}}\left[\frac{R_{90}(1+R_0)\sigma_x^2 - 2R_0R_{90}\sigma_x\sigma_y + R_0(1+R_{90})\sigma_y^2}{R_0+R_{90}+R_0R_{90}}\right]^{1/2}$$

$$\dot{\bar{\varepsilon}} = \sqrt{\frac{2}{3}\frac{R_0+R_{90}+R_0R_{90}}{R_0R_{90}(1+R_0+R_{90})}}\,[R_0(1+R_{90})D_{xx}^2 + 2R_0R_{90}D_{xx}D_{yy} + R_{90}(1+R_0)D_{yy}^2]^{1/2}. \tag{A3}$$

A linear straining path is characterized by the value of the strain rate ratio $\rho = D_{yy}/D_{xx}$ or by the value of the stress ratio $\alpha = \sigma_{yy}/\sigma_{xx}$, which are related by:

$$\rho = \frac{R_0(-R_{90}+\alpha+\alpha R_{90})}{R_{90}(1+R_0-R_0\alpha)}. \tag{A4}$$

In terms of these ratios (A3) reads:

$$\bar{\sigma} = \sigma_x\sqrt{\frac{3}{2}}\left[\frac{R_{90}(1+R_0) - 2R_0R_{90}\alpha + R_0(1+R_{90})\alpha^2}{R_0+R_{90}+R_0R_{90}}\right]^{1/2}$$

$$\dot{\bar{\varepsilon}} = D_{xx}\sqrt{\frac{2}{3}\frac{R_0+R_{90}+R_0R_{90}}{R_0R_{90}(1+R_0+R_{90})}}\,[R_0(1+R_{90}) + 2\rho R_0R_{90} + R_{90}(1+R_0)\rho^2]^{1/2}. \tag{A5}$$

For normal anisotropy ($R_0 = R_{45} = R_{90} = R$), the effective stress and effective strain rate are

$$\bar{\sigma} = \sqrt{\frac{3}{2}\frac{R+1}{R+2}}\left[\sigma_x^2 + \sigma_y^2 - \frac{2R}{1+R}\sigma_x\sigma_y\right]^{1/2}$$

$$\dot{\bar{\varepsilon}} = \sqrt{\frac{2}{3}\frac{(2+R)(1+R)}{1+2R}}\left[D_{xx}^2 + \frac{2R}{1+R}D_{xx}D_{yy} + D_{yy}^2\right]^{1/2} \tag{A6}$$

and the relation (A4) becomes

$$\rho = \frac{(\alpha+\alpha R-R)}{1+R-R\alpha}. \tag{A7}$$

APPENDIX B

In a non-deformable solid plate with adiabatic boundaries, the heat flow is governed by the heat conduction equation (conservation of calorific energy)

$$c\dot{\theta} = -\frac{1}{h}(hq_\alpha)_{,\alpha} \quad (\alpha = 1, 2) \tag{B1}$$

where h is the thickness of the plate. The heat flux vector $\mathbf{q}$ is given by Fourier's law, which reads for isotropic heat conductivity:

$$q_\alpha = -k\frac{\partial\theta}{\partial x_\alpha} \quad (\alpha = 1, 2). \tag{B2}$$

All quantities are average values through the plate thickness.

In a rigid (elastic deformations neglected) viscoplastic solid a part β of the plastic rate of work $\bar{\sigma}\dot{\bar{\varepsilon}}$ is converted into heat. The conservation of energy results in eqn (16).

APPENDIX C

The perturbed form of the flow law (10) is

$$\delta D_{11} = T_{11}\delta\dot{\bar{\varepsilon}} + \dot{\bar{\varepsilon}}\delta T_{11}$$

$$\delta D_{22} = T_{22}\delta\dot{\bar{\varepsilon}} + \dot{\bar{\varepsilon}}\delta T_{22}$$

$$\delta D_{12} = T_{12}\delta\dot{\bar{\varepsilon}} + \dot{\bar{\varepsilon}}\delta T_{12} \tag{C1}$$

with

$$\delta T_{ij} = \frac{\partial T_{ij}}{\partial \sigma_{kl}} \delta \sigma_{kl} = U_{ijkl} \frac{\delta \sigma_{kl}}{\bar{\sigma}} \tag{C2}$$

where the components of the fourth order tensor U are defined by:

$$U_{ijkl} = \bar{\sigma} \frac{\partial T_{ij}}{\partial \sigma_{kl}} = \bar{\sigma} \frac{\partial^2 \bar{\sigma}}{\partial \sigma_{ij} \partial \sigma_{kl}}. \tag{C3}$$

Using the relations (9), these components are, in the principal frame of anisotropy (x, y),

$$\begin{aligned}
U_{xxxx} &= \bar{\sigma} \frac{\partial T_{xx}}{\partial \sigma_{xx}} = \frac{3}{2} \frac{G+H}{F+G+H} - T_{xx}^2 \\
U_{xxyy} &= \bar{\sigma} \frac{\partial T_{xx}}{\partial \sigma_{yy}} = -\frac{3}{2} \frac{H}{F+G+H} - T_{xx} T_{yy} \\
U_{xxxy} &= \bar{\sigma} \frac{\partial T_{xx}}{\partial \sigma_{xy}} = -T_{xx} T_{xy} \\
U_{yyyy} &= \bar{\sigma} \frac{\partial T_{yy}}{\partial \sigma_{yy}} = \frac{3}{2} \frac{H+F}{F+G+H} - T_{yy}^2 \\
U_{yyxy} &= \bar{\sigma} \frac{\partial T_{yy}}{\partial \sigma_{xy}} = -T_{yy} T_{xy} \\
U_{xyxy} &= \bar{\sigma} \frac{\partial T_{xy}}{\partial \sigma_{xy}} = \frac{3}{2} \frac{N}{F+G+H} - T_{xy}^2.
\end{aligned} \tag{C4}$$